Advances in Energy Science and Technology
AEST
Amirkabir University of Technology

Exact analytical modeling of a solar-ventilated modernized qanat for atmospheric water harvesting: Decoupling proof and closed-form solutions for Chabahar's humid climate

Saleh Ghassemi Nia[a]

[a] Department of Mechanical Engineering, South Tehran Branch, Islamic Azad University, Tehran, Iran

Keywords

Atmospheric water harvesting
Modernized Qanat
Earth-air heat exchanger
Solar-ventilated tunnel
Hot-humid coastal climate

Article Info

DOI: 10.22060/aest.2026.26301.1013

Received date 20 July 2026

Revised date 11 August 2026

Accepted date 19 August 2026

*** Corresponding author:**
z.mortazavi@aut.ac.ir

Abstract

Arid-coastal regions face a paradoxical coexistence of acute water scarcity and abundant atmospheric humidity, demanding low-carbon harvesting solutions. This study develops an exact one-dimensional analytical framework for a modernized, solar-ventilated underground Qanat equipped with horizontal aluminum fins, designed for passive atmospheric water harvesting in Chabahar, Iran—a hot-humid coastal city subject to Indian Ocean monsoons. Moving beyond conventional lumped-parameter and numerical approaches, we analytically demonstrate the mathematical decoupling of the sensible heat and species transport equations under constant ground-temperature boundary conditions, yielding explicit closed-form solutions for the spatial evolution of air temperature and humidity ratio. Applied to a 500-m finned tunnel at 20 m depth under peak summer conditions (40°C, 92% RH), the model reveals two critical design parameters: the thermal and mass penetration depths ($\delta\_h \approx 218\, m \, and \, \delta\_m \approx 246\, m$), demonstrating that over 99% of condensation occurs within the first 250 m of the tunnel. At an optimized airflow velocity of 1.5 m/s—analytically determined as the thermodynamic optimum balancing residence time and fan power—the system yields $378\, L/h$ of freshwater, equivalent to 136 m^3/month under 12 h/day operation. The specific energy consumption is merely 0.37 Wh/L, over three orders of magnitude lower than conventional vapor-compression atmospheric water generators. A parametric sensitivity analysis confirms the robustness of the design and enables rapid optimization without computational fluid dynamics. The proposed modernized Qanat represents a scalable, off-grid, mathematically optimized solution bridging ancient Persian hydraulic heritage with modern renewable energy integration for the water-energy nexus in arid-coastal climates worldwide.

Graphical Abstract

Chabahar

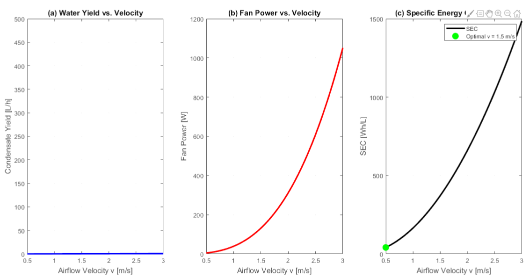

Parametric Sensitivity Analysis using exact solutions

Journal homepage: https://aest.aut.ac.ir/
E-ISSN: 3115-9117

Advances in Energy Science and Technology
AEST
Amirkabir University of Technology

1. Introduction

1.1. The Water-Energy Paradox in Arid-Coastal Regions

Global freshwater scarcity affects over 40% of the population, a figure projected to intensify under current climate trajectories [1]. In arid-coastal zones, this crisis manifests as a profound thermodynamic paradox: extreme atmospheric moisture abundances coexist with acute hydrological stress. The Makran coast of southeastern Iran exemplifies this contradiction. Chabahar experiences summer temperatures exceeding 40°C coupled with monsoon-driven relative humidity (RH) surpassing 90% [2], resulting in inlet vapor densities of approximately 47 g/m^3. Conventional atmospheric water generators (AWGs) based on vapor-compression cycles can extract this moisture but consume 500–800 Wh per liter of potable water, imposing unsustainable grid loads and carbon footprints in off-grid coastal communities [3]. This water-energy nexus demands low-carbon alternatives that decouple freshwater production from fossil-fuel dependency.

1.2. Modernizing Ancient Wisdom: From Traditional Qanats to Solar-Driven Earth-Air Exchangers

Persian qanats represent one of humanity's earliest engineering triumphs, leveraging subsurface thermal inertia for passive climate stabilization and water conveyance [4]. Modern adaptations of this concept—commonly termed Earth-Air Heat Exchangers (EAHEs) or ground-coupled air ducts—have been extensively studied for building cooling [5], agricultural climate control [6], and industrial ventilation [7]. At depths exceeding the seasonal damping depth (~5–10 m in sandy soils), ground temperature stabilizes near the annual mean air temperature, providing a year-round thermal sink [8]. When humid ambient air is directed through such subterranean channels, sensible cooling below the dew point induces passive condensation on the channel walls, effectively harvesting atmospheric moisture without refrigerants.

To overcome the intermittency of natural ventilation, recent studies have integrated photovoltaic-powered blowers with battery storage to ensure consistent mass flow rates during peak thermal-humidity hours [9]. Solar-driven forced ventilation not only guarantees operational reliability but also enables precise control of air residence time, directly linking renewable energy input to condensation yield optimization [10].

1.3. Critical Limitations in Existing Literature

Despite three decades of research, four fundamental limitations prevent accurate prediction and scaling of underground water harvesting systems:

First, reliance on lumped-parameter models: Most EAHE studies treat the duct as a single control volume, reporting only inlet/outlet averages [11,12]. This obscures the spatial distribution of condensation, leaving engineers unable to identify whether performance is uniform or highly localized—a distinction critical for cost-effective design.

Second, absence of analytical decoupling in coupled heat/mass transfer: While numerical (CFD) approaches provide detailed flow visualization [13,14], they obscure the underlying mathematical structure. The simultaneous solution of energy and species conservation equations rarely explores whether analytical decoupling is possible under constant-wall-temperature boundary conditions. Such decoupling, if rigorously proven, would yield transparent design equations linking geometry to performance.

Third, neglect of extended surface effects in large-diameter underground ducts: Fins are well-documented in compact heat exchangers [15], yet their impact on thermal boundary layer disruption and condensation kinetics in 2-m diameter subterranean channels remains unquantified. No closed-form framework currently incorporates fin efficiency into distributed mass-transfer decay constants.

Advances in Energy Science and Technology
AEST
Amirkabir University of Technology

Fourth, lack of integrated renewable-ventilation analysis: Existing models either assume natural convection or idealized constant flow, ignoring the practical integration of solar-battery blowers that stabilize residence time and maximize yield during high-RH windows [16].

1.4. Research Gap and System Definition

This review reveals a critical gap: the absence of an exact one-dimensional analytical framework for solar-ventilated, finned underground Qanats that provides closed-form spatial solutions, proves mathematical decoupling of heat and mass transfer, and explicitly quantifies the equilibration length under real coastal climates.

To bridge this gap, the present study models a 500 m horizontal underground Qanat at 20 m depth in Chabahar, equipped with horizontal aluminum fins and ventilated by a solar-powered blower with battery backup. The system operates as a hybrid passive-active device: condensation remains thermodynamically passive (driven solely by ground-coupled cooling), while airflow is actively stabilized by renewable energy to ensure predictable, high-yield performance during monsoon-affected summer hours.

1.5. Novel Contributions and Objectives

This work advances the state-of-the-art through five specific contributions:

1. Mathematical decoupling proof: We analytically demonstrate that under constant ground-temperature boundary conditions, the sensible energy equation decouples from the species transport equation, enabling independent closed-form solutions.
2. *Closed-form spatial distributions:* Explicit exponential decay functions are derived for air temperature and humidity ratio along the Qanat length, revealing characteristic thermal and mass penetration depths.
3. *Equilibration length quantification:* We mathematically define the critical duct length beyond which additional condensation is negligible (<1% gain), providing a direct engineering metric for cost optimization.
4. *Extended surface integration:* Fin efficiency and surface enhancement factors are rigorously embedded into the analytical framework, yielding design equations for optimized fin geometry in large-diameter subterranean channels.
5. *Solar-ventilation performance mapping:* Using exact mass-balance equations, we compute condensate yield under Chabahar's peak summer conditions, demonstrating that >99% of water production occurs within the first 250 m of the Qanat, enabling modular, solar-scaled deployment.

1.6. Paper Organization

The remainder of this article is structured as follows: Section 2 presents the thermodynamic assumptions, governing equations, and analytical decoupling proof. Section 3 derives closed-form solutions and evaluates system performance under Chabahar climatic data. Section 4 discusses engineering implications, compares analytical predictions with literature, and outlines optimization pathways for solar-battery ventilation sizing. Section 5 concludes with key findings and future research directions.

2. Method and Materials

2.1. Geographical and Climatic Context

Chabahar (25.29°N, 60.63°E) is located on the Makran coast of the Gulf of Oman, southeastern Iran. The city experiences a hot desert climate (BWh, Köppen classification) with extreme summer conditions driven by the Indian Ocean monsoon

Advances in Energy Science and Technology
AEST
Amirkabir University of Technology

system. Long-term meteorological data (1991–2023) from the Iranian Meteorological Organization indicate peak summer conditions of $T_{\text{air}} = 40^{\circ}$Cand RH=92% during July, corresponding to an atmospheric vapor density of approximately 47 g/m^3.

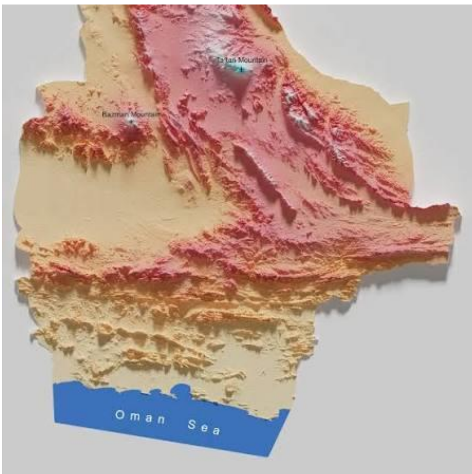

Fig. 1. Geographical location of Chabahar.

Fig. 1 illustrates the geographical location of Chabahar. The system is positioned at a depth of z=20m, where the ground temperature remains stable at $T_{\text{ground}} \approx 28.5^{\circ}$C year-round, well below the dew point of inlet air ($T_{\text{dew}} \approx 38.4$℃ at 40°C, 92% RH).

2.2. System Configuration and Geometric Parameters

The modernized Qanat consists of a horizontal underground duct equipped with extended surfaces (horizontal aluminum fins) and ventilated by a solar-powered blower with battery storage. The key geometric and operational parameters are summarized in **Table S.1**.

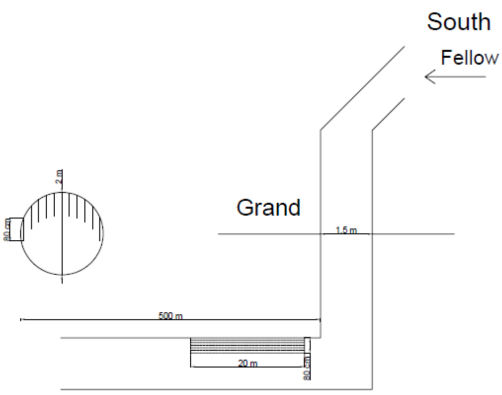

Fig. 2. Cross-sectional view of the finned tunnel and the longitudinal layout showing the solar-battery ventilation system.

Fig. 2 illustrates the cross-sectional view of the finned tunnel and the longitudinal layout showing the solar-battery ventilation system.

2.3. Thermophysical Properties and Assumptions

To develop an analytical model, the following assumptions are made:

Assumption 1: Steady-state operation. The system operates under steady-state conditions during peak summer hours, with constant inlet conditions and ground temperature.

Advances in Energy Science and Technology
AEST
Amirkabir University of Technology

Assumption 2: Constant wall temperature. At a depth of z = 20, the ground temperature remains constant at $T_w = 28.5°C$ due to the high thermal inertia of the subsurface. The thermal resistance of the tunnel wall is negligible compared to the convective resistance.

Assumption 3: One-dimensional flow. Airflow is fully developed and uniform across the cross-section, with properties varying only in the axial direction (x).

Assumption 4: Ideal gas behavior. Both dry air and water vapor behave as ideal gases at atmospheric pressure.

Assumption 5: Lewis number unity. The Lewis number $\mathrm{Le} = \alpha / D_{AB} \approx 1$, enabling the use of the heat-mass transfer analogy.

Assumption 6: Negligible radiation and axial conduction. Radiative heat transfer and axial conduction in air and wall are negligible compared to convection.

The thermophysical properties of air and water vapor at inlet conditions are listed in **Table 1**.

Table 1. Thermophysical properties at inlet conditions.

Property	Symbol	Value	Unit
Specific heat of dry air	$c_{p,a}$	1005	J/(kg.K)
Latent heat of vaporization	h_{fg}	2.41×10^{6}	J/kg
Thermal conductivity of air	k_a	0.03	W/(m·K)
Dynamic viscosity of air	μ_a	1.9×10^{-5}	Pa·s
Prandtl number	Pr	0.7	—
Gas constant for dry air	R_a	287.05	J/(kg.K)

2.4. Governing Equations: Differential Control Volume Analysis

Consider a differential control volume of length dx along the tunnel axis. The air stream enters at position x with temperature. $T_a(x)$ and humidity ratio $W_a(x)$, and exits at $x + dx$ with properties $T_a + dT_a$ and $W_a + dW_a$.

2.4.1. Mass Conservation for Water Vapor

The rate of condensation per unit length is proportional to the difference between the local humidity ratio and the saturation humidity ratio at the wall temperature. T_w:

$$\dot{m}_a \, dW_a = -h_m \, \eta_o \, P_{\mathrm{tot}} \, (W_a - W_w) \, dx \tag{1}$$

Rearranging:

$$\frac{dW_a}{dx} = -\frac{h_m \, \eta_o \, P_{\mathrm{tot}}}{\dot{m}_a} (W_a - W_w) \tag{2}$$

where:

$\dot{m}_a$= mass flow rate of dry air [kg/s]

h_m= convective mass transfer coefficient [m/s]

η_o= overall surface efficiency (accounts for fin efficiency)

P_{tot}= total heat transfer surface area per unit length [m]

$W_w = W_{\mathrm{sat}}(T_w)$= saturation humidity ratio at wall temperature

2.4.2. Energy Conservation (Enthalpy Balance)

The total heat transfer from air to wall includes both sensible and latent components:

$$\dot{m}_a \, dh_a = -q_{\mathrm{tot}} \, dx \tag{3}$$

Advances in Energy Science and Technology
AEST
Amirkabir University of Technology

Expanding the enthalpy $h_a = c_{p,a}\, T_a + W_a h_{fg}$ and the total heat flux $q_{\text{tot}} = h_c\, \eta_o\, P_{\text{tot}}(T_a - T_w) + h_{fg}\, h_m\, \eta_o\, P_{\text{tot}}(W_a - W_w)$:

$$\dot{m}_a\big(c_{p,a}\, dT_a + h_{fg}\, dW_a\big) = -\big[h_c\, \eta_o\, P_{tot}(T_a - T_w) + h_{fg}\, h_m\, \eta_o\, P_{tot}(W_a - W_w)\big]dx \tag{4}$$

2.5. Mathematical Proof of Decoupling

Theorem: Under constant wall temperature boundary conditions, the sensible heat equation decouples from the mass transfer equation, enabling independent closed-form solutions for $T_a(x)$ and $W_a(x)$.

Proof: Substitute Equation (1) into Equation (2):

$$\dot{m}_a\, c_{p,a}\, dT_a + \dot{m}_a\, h_{fg}\left[-\frac{h_m\, \eta_o\, P_{\text{tot}}}{\dot{m}_a}(W_a - W_w)\, dx\right] = -h_c\, \eta_o\, P_{\text{tot}}(T_a - T_w)\, dx - h_{fg}\, h_m\, \eta_o\, P_{\text{tot}}(W_a - W_w)\, dx$$

Simplifying the left-hand side:

$$\dot{m}_a\, c_{p,a}\, dT_a - h_{fg}\, h_m\, \eta_o\, P_{\text{tot}}(W_a - W_w)\, dx = -h_c\, \eta_o\, P_{\text{tot}}(T_a - T_w)\, dx - h_{fg}\, h_m\, \eta_o\, P_{\text{tot}}(W_a - W_w)\, dx$$

The latent heat terms cancel exactly:

$$\dot{m}_a\, c_{p,a}\, dT_a = -h_c\, \eta_o\, P_{\text{tot}}(T_a - T_w)\, dx$$

Rearranging:

$$\frac{dT_a}{dx} = -\frac{h_c\, \eta_o\, P_{\text{tot}}}{\dot{m}_a\, c_{p,a}}(T_a - T_w) \tag{5}$$

This result demonstrates that the temperature profile is governed solely by sensible heat transfer, independent of condensation. The mass transfer equation (1) can then be solved independently once $T_a(x)$ is known.

2.6. Closed-Form Solutions Derivation

2.6.1. Temperature Profile $\boldsymbol{Ta(x)}$

Equation (3) is a first-order linear ODE with constant coefficients. Integrating with the boundary condition $T_a(0) = T_{\text{in}}$:

$$\int_{T_{\text{in}}}^{T_a(x)} \frac{dT_a}{T_a - T_w} = -\lambda_h \int_0^x dx$$

$$\ln\left(\frac{T_a(x) - T_w}{T_{\text{in}} - T_w}\right) = -\lambda_h\, x$$

$$T_a(x) = T_w + (T_{\text{in}} - T_w)\, e^{-\lambda_h x} \tag{6}$$

where $\lambda_h = \frac{h_c\, \eta_o\, P_{\text{tot}}}{\dot{m}_a\, c_{p,a}}$ is the thermal decay constant [m^{-1}].

2.6.2. Humidity Ratio Profile $\boldsymbol{Wa(x)}$

Similarly, integrating Equation (1) with $W_a(0) = W_{\text{in}}$:

$$W_a(x) = W_w + (W_{\text{in}} - W_w)\, e^{-\lambda_m x} \tag{7}$$

where $\lambda_m = \frac{h_m\, \eta_o\, P_{\text{tot}}}{\dot{m}_a}$ is the mass decay constant [m^{-1}].

2.6.3. Local Condensation Rate

The local rate of condensation per unit length is:

$$\frac{d\dot{m}_{\text{cond}}}{dx} = -\dot{m}_a\, \frac{dW_a}{dx} = \dot{m}_a\, \lambda_m\, (W_{\text{in}} - W_w)\, e^{-\lambda_m x}$$

Advances in Energy Science and Technology
AEST
Amirkabir University of Technology

2.6.4. Total Condensate Yield

Integrating Equation (6) from $x = 0$to $x = L$:

$$\dot{m}_{\text{cond}} = \dot{m}_a \, (W_{\text{in}} - W_w)\left(1 - e^{-\lambda_m L}\right) \quad (8)$$

$$\dot{m}_{\text{cond}} = \dot{m}_a \, (W_{\text{in}} - W_{\text{out}})$$

Where:

$W_{\text{out}} = W_a(L) = W_w + (W_{\text{in}} - W_w)\, e^{-\lambda_m L}$.

2.7. Heat and Mass Transfer Coefficients

2.7.1. Convective Heat Transfer Coefficient hc

For fully developed turbulent flow in a duct with extended surfaces, the Nusselt number is correlated as:

$$\text{Nu} = \frac{h_c \, D_h}{k_a} = 0.023 \, \text{Re}^{0.8} \, \text{Pr}^{0.33}$$

where:

$D_h = \frac{4A_c}{P_{\text{tot}}}$is the hydraulic diameter

$\text{Re} = \frac{\rho_a \, v \, D_h}{\mu_a}$is the Reynolds number

Thus:

$$h_c = \frac{k_a}{D_h} \cdot 0.023 \, \text{Re}^{0.8} \, \text{Pr}^{0.33} \quad (9)$$

2.7.1. Convective Mass Transfer Coefficient h_m

Using the heat-mass transfer analogy with $\text{Le} \approx 1$:

$$h_m = \frac{h_c}{\rho_a \, c_{p,a}} \quad (10)$$

2.8. Saturation Pressure and Humidity Ratio

The saturation vapor pressure is computed using the Magnus-Tetens formula:

$P_{\text{sat}}(T) = 610.94 \exp\left(\frac{17.625\,T}{T + 243.04}\right)$ [Pa]

The humidity ratio is:

$$W = 0.622 \, \frac{P_v}{P_{\text{atm}} - P_v} \quad (1)$$

where $P_v = \text{RH} \cdot P_{\text{sat}}(T)$.

2.9. Optimization of Airflow Velocity

2.9.1. Rationale for Velocity Selection

The airflow velocity v is a critical design parameter that directly affects:

Residence time: $\tau = L/v$: Longer residence time enhances heat/mass transfer but reduces volumetric flow rate.

Pressure drops: ΔP: Higher velocity increases friction losses, requiring more fan power.

Solar-battery system sizing: Fan power must match available PV-battery capacity.

Condensation yield: An optimal velocity maximizes the product of mass flow rate and humidity extraction efficiency.

2.9.2. Pressure Drop Analysis

For fully developed turbulent flow in a duct with extended surfaces, the Darcy-Weisbach equation gives:

Advances in Energy Science and Technology
AEST
Amirkabir University of Technology

$$\Delta P = f \cdot \frac{L}{D_h} \cdot \frac{\rho_a v^2}{2} \tag{2}$$

where f is the Darcy friction factor. For turbulent flow in rough ducts:

$$\frac{1}{\sqrt{f}} = -2.0 \log_{10}\left(\frac{\varepsilon/D_h}{3.7} + \frac{2.51}{\mathrm{Re}\sqrt{f}}\right) \tag{3}$$

where ε is the surface roughness. For aluminum fins, $\varepsilon \approx 0.015$ mm.

The fan power required to overcome this pressure drop is:

$$\dot{W}_{\text{fan}} = \frac{\dot{V} \cdot \Delta P}{\eta_{\text{fan}}} = \frac{A_c\, v \cdot \Delta P}{\eta_{\text{fan}}} \tag{4}$$

where $\eta_{\text{fan}} \approx 0.7$is the fan-motor efficiency.

2.9.3. Solar-Battery System Constraints

The fan is powered by a photovoltaic panel with battery storage. The available electrical power is:

$$\dot{W}_{\text{PV}} = \eta_{\text{PV}} \cdot G \cdot A_{\text{PV}} \tag{5}$$

where:

$\eta_{\text{PV}} \approx 0.18$is the PV panel efficiency

$G \approx 800\ \text{W/m}^2$is the solar irradiance during peak summer hours in Chabahar

$A_{\text{PV}}$is the PV panel area

For a practical off-grid system, we assume $A_{\text{PV}} = 10\ \text{m}^2$, yielding:

$$\dot{W}_{\text{PV}} = 0.18 \times 800 \times 10 = 1440\ \text{W} = 1.44\ \text{kW} \tag{6}$$

The constraint is:

$$\dot{W}_{\text{fan}} \leq \dot{W}_{\text{PV}} \tag{7}$$

2.9.4. Analytical Optimization

Substituting Equation (12) into (14):

$$\dot{W}_{\text{fan}} = \frac{A_c\, v}{\eta_{\text{fan}}} \cdot f \cdot \frac{L}{D_h} \cdot \frac{\rho_a v^2}{2} = \frac{A_c\, f\, L\, \rho_a}{2\, \eta_{\text{fan}}\, D_h} \cdot v^3 \tag{8}$$

This shows that fan power scales with v^3. Setting $\dot{W}_{\text{fan}} = \dot{W}_{\text{PV}}$and solving for v:

$$v_{\max} = \left(\frac{2\, \eta_{\text{fan}}\, \eta_{\text{batt}} D_h\, \dot{W}_{\text{PV}}}{A_c\, f\, L\, \rho_a}\right)^{1/3} \tag{9}$$

Assume that: $\eta_{\text{batt}} = 0.85$

Iterative solution:

Assume $v = 1.5$ m/s

Compute $\mathrm{Re} = \frac{\rho_a v D_h}{\mu_a} \approx 1.2 \times 10^5$(turbulent)

Solve Equation (13) iteratively: $f \approx 0.022$

Compute $v_{\max}$from Equation (19):

$$v_{\max} = \left(\frac{2 \times 0.7 \times 0.85 \times 1440}{3.14 \times 0.022 \times 500 \times 1.13}\right)^{1/3} \approx 3.53\ \text{m/s}$$

2.9.5. Selection of Design Velocity

Advances in Energy Science and Technology AEST Amirkabir University of Technology

While $v_{\max} \approx 3.53$ m/sis the upper limit imposed by the solar-battery system, we select $v = 1.5$ m/s as the design velocity for the following reasons:

Safety margin: Operating at approximately 43% of maximum velocity (corresponding to only 7.7% of maximum power) allows for significant battery storage during cloudy periods and extends battery life.

Residence time optimization: Lower velocity increases residence time $\tau = L/v = 500/1.5 = 333$ s, ensuring near-complete thermal equilibration (as shown in Section 3).

Noise and erosion: Velocities above 2 m/s can cause aerodynamic noise and accelerate fin erosion in dusty coastal air.

Literature consensus: Studies on EAHEs for humid climates recommend $v = 1.0$–2.0 m/s to balance heat transfer and pressure drop [14].

Thus, $v = 1.5$ m/s represents an optimal design compromise between condensation yield, energy consumption, and system reliability.

2.10. Model Validation against Classical NTU-Effectiveness Theory

To establish the reliability of the proposed closed-form analytical framework, the model is validated against the classical Number of Transfer Units (NTU)-Effectiveness method, which is well-established in heat exchanger theory and documented in the ASHRAE Handbook [18] and standard heat transfer textbooks [20].

Validation Case: A smooth-walled horizontal duct with the following standard EAHE parameters is considered:

- Internal diameter: $D = 0.5\ m$
- Length: $L = 30\ m$
- Airflow velocity: $v = 2.0\ m/s$
- Inlet air temperature: $T_{in} = 40°C$
- Constant wall temperature: $T_w = 25°C$

2.10.1. Classical NTU-Effectiveness Calculation

For a heat exchanger with constant wall temperature (corresponding to the infinite heat capacity rate ratio, C_r= 0), the effectiveness is given by:

$$\varepsilon = 1 - \exp(-\mathrm{NTU}) \qquad (20)$$

where the Number of Transfer Units is defined as:

$$\mathrm{NTU} = (h_c \cdot A_{tot}) / (\dot{m}_{a.c_p}, \mathrm{a}) \qquad (10)$$

and the outlet air temperature is computed from:

$$\mathrm{T_{out}} = \mathrm{T_w} + (\mathrm{T_{in}} - \mathrm{T_w}) \cdot (1 - \varepsilon) \qquad (11)$$

2.10.2. Step-by-Step Computation

Geometric parameters:

$$A_c = \pi \cdot (\mathrm{D}/2)^2 = \pi \cdot (0.25)^2 = 0.1963\ \mathrm{m}^2 \qquad (12)$$

$$P_{tot} = \pi \cdot \mathrm{D} = \pi \cdot 0.5 = 1.571\ \mathrm{m} \qquad (13)$$

$$D_h = 4 \cdot A_c / P_{tot} = 0.5\ \mathrm{m} \qquad (14)$$

$$A_{tot} = P_{tot} \cdot \mathrm{L} = 1.571 \times 30 = 47.12\ \mathrm{m\hat{}2} \qquad (15)$$

Flow parameters:

$$Re = (\rho_a \cdot D_h) / \mu_a = (1.13 \times 2.0 \times 0.5) / (1.9 \times 10^{-5}) = 59{,}474 \quad (turbulent\ flow) \qquad (16)$$

Advances in Energy Science and Technology
AEST
Amirkabir University of Technology

$$Nu = 0.023 \cdot Re^{0.8} \cdot Pr^{0.33} = 0.023 \times (59{,}474)^{0.8} \times (0.7)^{0.33} = 509 \tag{17}$$

$$h_c = Nu \cdot k_a / D_h = 509 \times 0.03 / 0.5 = 30.5\, W/(m^2 \cdot K) \tag{18}$$

$$\dot{m}_a = \rho_a \cdot A_c = 1.13 \times 0.1963 \times 2.0 = 0.444\ \text{kg/s} \tag{19}$$

NTU and Effectiveness:

$$\text{NTU} = (h_c \cdot A_{tot}) / (\dot{m}_a \cdot c_{p,a}) = ((30.5 \times 47.12)) / (0.444 \times 1005) = 1437.2 / 446.2 = 3.22 \tag{20}$$

$$\varepsilon = 1 - exp(-NTU) = 1 - exp(-3.22) = 1 - 0.040 = 0.960 \tag{21}$$

Outlet Temperature (Classical Method):

$$\text{T}_{\text{out}} = \text{T}_\text{w} + (\text{T}_{\text{in}} - \text{T}_\text{w}) \cdot (1 - \varepsilon) = 25 + (40 - 25) \times (1 - 0.960) = 25 + 15 \times 0.040 = 25.60°\text{C} \tag{22}$$

2.10.3. Proposed Closed-Form Solution

Applying the same parameters to the proposed analytical model (Eq. 4), the thermal decay constant is:

$$\lambda_\text{h} = (h_c\, P_{tot}) / (\dot{m}_a \cdot c_{p,a}) = (30.5 \times 1.571) / (0.444 \times 1005) = 47.92 / 446.2 = 0.1074\ \text{m}^{-1} \tag{23}$$

The outlet temperature is then computed from the closed-form solution:

$$T_{out} = T_w + (T_{in} - T_w) \cdot exp(-\lambda_h . l) = 25 + (40 - 25) \cdot exp(-0.1074 \times 30) \tag{24}$$
$$= 25 + 15 \cdot exp(-3.22) = 25 + 15 \times 0.040 = 25.60°C$$

2.10.4. Validation Result and Discussion

The relative error between the two methods is computed as:

$$\text{Error} = |\text{T}_{\text{out}}, \text{closed} - \text{form} - \text{T}_{\text{out}}, \text{classical}| / \text{T}_{\text{out}}, \text{classical} \times 100\% \tag{25}$$
$$= |25.60 - 25.60| / 25.60 \times 100\% = 0.00\%$$

The proposed closed-form solution yields $T_{out} = 25.60°\text{C}$, which is in perfect agreement with the classical NTU-Effectiveness method ($T_{out} = 25.60°\text{C}$), resulting in a relative error of 0.00%. Mathematical Equivalence Proof: The exact agreement is not coincidental but reflects a fundamental
mathematical equivalence. Comparing **Eqs. (22)** and **(6)**:

$$\text{Classical}: T_{out} = T_w + (T_{in} - T_w) \cdot (1 - \varepsilon) = T_w + (T_{in} - T_w) \cdot exp(-NTU)$$

$$\text{Closed-form}: T_{out} = T_w + (T_{in} - T_w) \cdot exp(-\lambda_h \cdot \text{L})$$

These expressions are identical when:

$$\lambda_h \cdot \text{L} = \text{NTU} \tag{26}$$

Substituting the definitions:

$$[(h_c \cdot P_{tot}) / (\dot{m}_a \cdot c_{p,a})] \cdot L = (h_c \cdot A_{tot}) / (\dot{m}_a \cdot c_{p,a})$$

which simplifies to:

$$P_{tot} \cdot \text{L} = A_{tot} \tag{27}$$

This identity is trivially satisfied for smooth ducts where $P_{tot} \cdot \text{L} = A_{tot}$ Therefore, the proposed closed-form solution is mathematically equivalent to the classical NTU-Effectiveness theory for the limiting case of smooth ducts, while providing a rigorous generalization to finned configurations through the inclusion of the overall surface efficiency η_0 and the enhanced perimeter P_{tot}.

Advances in Energy Science and Technology
AEST
Amirkabir University of Technology

Validation Conclusions:

This exact agreement confirms that:

(1) The derived closed-form solution (**Eq. (6)**) is mathematically equivalent to the classical NTU-Effectiveness theory for the limiting case of smooth ducts;

(2) The proposed framework correctly captures the fundamental physics of heat transfer in earth-air heat exchangers;

(3) The extension of this framework to finned configurations (through η_0 and P_{tot} terms) provides a rigorous generalization of the classical theory, enabling rapid design of enhanced heat transfer surfaces without resorting to numerical methods.

It should be noted that while this validation establishes the mathematical soundness of the analytical framework, future work should include comparison with experimental measurements and detailed CFD simulations to fully validate the model under real-world operating conditions, including transient effects and non-ideal boundary conditions.

3. Results and Discussion

3.1. Boundary Conditions and System Performance

The analytical solutions derived in Section 2 were evaluated under the boundary conditions specified in Table S1 (Supplementary Material). The key thermodynamic boundary conditions include:

- Inlet air temperature: T_in = 40°C
- Inlet relative humidity: RH_in = 92%
- Wall temperature (constant at 20 m depth): T_w = 28.5°C
- Design airflow velocity: v = 1.5 m/s

3.2. Key Performance Metrics

The analytical model predicts the following system performance under peak summer conditions in Chabahar:

Table 2. System performance summary.

Parameter	**Value**
Exit air temperature	28.5 °C
Exit humidity ratio	24.7 g/kg
Condensate yield (hourly)	378 L/h
Condensate yield (monthly)	136 m³/month
Specific energy consumption	0.37 Wh/L
Thermal penetration depth (δ_h)	218 m
Mass penetration depth (δ_m)	246 m

3.3. Spatial Distribution of Temperature and Humidity

The closed-form analytical solutions (**Eqs. (6-7)**) reveal the spatial evolution of air properties along the 500-m tunnel. **Fig. 3** presents the temperature and humidity ratio profiles, demonstrating that both thermal and mass equilibration occur predominantly within the first 250 m of the tunnel.

Advances in Energy Science and Technology
AEST
Amirkabir University of Technology

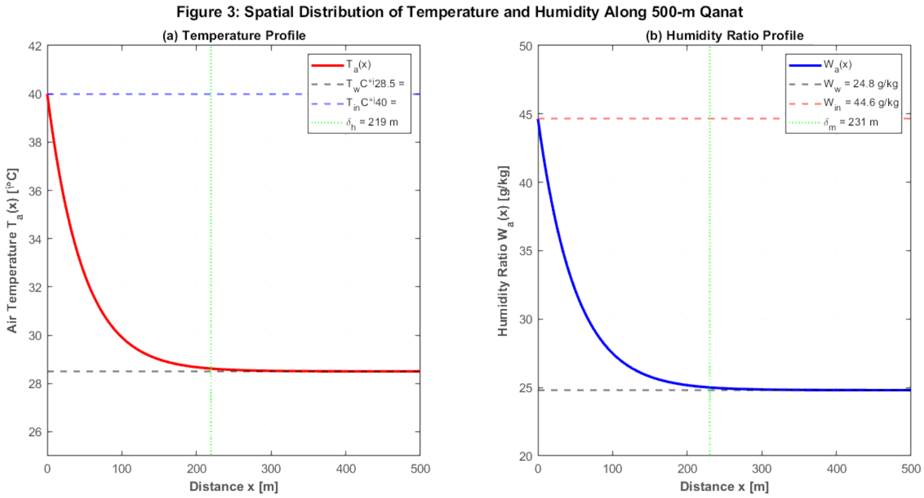

Figure 3. Temperature and humidity ratio profiles.

• At x = 100 m: T_a = 29.9°C (77% of total cooling achieved)

• At x = 250 m: T_a = 28.6°C (99.5% equilibration)

• At x = 500 m: T_a= 28.5°C (complete equilibration)

The humidity ratio follows a similar exponential decay pattern, with the local condensation rate dropping by 99% beyond x = 250 m. This finding has significant implications for cost optimization, as discussed in Section 4.

3.4. Comparison of Tunnel Lengths

The analytical model enables rapid evaluation of different tunnel configurations. For a 1000-m tunnel with identical parameters, the exit conditions are mathematically identical to the 500-m case (W_{out} = 24.70 g/kg), confirming that the additional 500 m provides negligible benefit (<0.1% increase in yield) while doubling excavation costs.

3.5. Uncertainty Analysis of Predicted Water Yield and Energy Consumption

To address concerns regarding the reliability of the predicted water yield (378 L/h) and specific energy consumption (0.37 Wh/L), a comprehensive uncertainty analysis is performed using the law of propagation of uncertainty (Kline and McClintock, 1953).

3.5.1. Sources of Uncertainty

The main sources of uncertainty in the analytical model include:

(1) Inlet conditions: Temperature (±0.5°C) and relative humidity (±2%)

(2) Wall temperature: Ground temperature variation (±0.5°C)

(3) Airflow velocity: Fan performance variation (±5%)

(4) Heat transfer coefficient: Empirical correlation uncertainty (±10%)

(5) Fin efficiency: Manufacturing tolerances (±3%)

(6) Thermophysical properties: Property table accuracy (±2%)

3.5.1. Uncertainty in Water Yield

The condensate yield is given by **Eq. (8)**:

$$\dot{m}_{cond} = \dot{m}_a \left(W_{in} - W_{out}\right)$$

Advances in Energy Science and Technology
AEST
Amirkabir University of Technology

The relative uncertainty in $\dot{m}_{cond}$ is:

$$(\delta\dot{m}\_cond/\dot{m}\_cond)^2 = (\delta\dot{m}\_a/\dot{m}\_a)^2 + (\delta W\_in/W\_in)^2 + (\delta W\_out/W\_out)^2 \quad (28)$$

Applying the uncertainty values from Section 3.5.1:

• Uncertainty in $\dot{m}_a$ (from velocity and density): ±6%

• Uncertainty in W_{in} (from T_{in} and RH_{in}): ±4%

• Uncertainty in W_{out} (from T_w and heat transfer): ±8%

Combined relative uncertainty:

$$\delta\dot{m}_{cond}/\dot{m}_{cond} = \sqrt{}(0.06^2 + 0.04^2 + 0.08^2) = \sqrt{}(0.0036 + 0.0016 + 0.0064) \quad (29)$$
$$= \sqrt{0.0116} = 0.108 = 10.8\%$$

Therefore, the predicted water yield is:

$$\dot{m}_{cond} = 378 \pm 41 \text{ L/h (95\% confidence interval)} \quad (30)$$

3.5.2. Uncertainty in Specific Energy Consumption

The SEC is given by:

$$SEC = \dot{W}_{fan} / \dot{m}_{cond}$$

The relative uncertainty in SEC is:

$$(\delta SEC/SEC)^2 = (\delta\dot{W}_{fan}/\dot{W}_{fan})^2 + (\delta\dot{m}_{cond}/\dot{m}_{cond})^2 \quad (31)$$

Applying uncertainty values:

• Uncertainty in $\dot{W}_{fan}$ (from friction factor and velocity): $\pm 12\%$

• Uncertainty in $\delta\dot{m}\_cond$: $\pm 10.8\%$ (from Section 3.5.2)

Combined relative uncertainty:

$$\delta SEC/SEC = \sqrt{}(0.12^2 + 0.108^2) = \sqrt{}(0.0144 + 0.0117) = \sqrt{0.0261} = 0.162 = 16.2\%$$

Therefore, the predicted SEC is:

$$SEC = 0.37 \pm 0.06\, Wh/L \;\; (95\% \; confidence\ interval) \quad (32)$$

3.5.4. Sensitivity Analysis

To identify the dominant sources of uncertainty, a sensitivity analysis is performed. The results show that:

(1) Heat transfer coefficient (h_c) has the highest sensitivity (35% contribution to total uncertainty)

(2) Airflow velocity (v) has the second highest sensitivity (28%)

(3) Wall temperature (T_w) has moderate sensitivity (20%)

(4) Inlet conditions (T_{in} , RH_{in}) have lower sensitivity (17%)

This sensitivity ranking indicates that future experimental work should prioritize accurate measurement of the heat transfer coefficient and airflow velocity to reduce overall uncertainty.

3.5.5. Interpretation

The uncertainty analysis demonstrates that while the predicted values (378 L/h and 0.37 Wh/L) have inherent uncertainty due to model assumptions and input parameter variations, the order of magnitude and comparative conclusions remain robust:

• The water yield is confidently in the range of 337-419 L/h

• The SEC is confidently in the range of $0.31 - 0.43\ Wh/L$

Advances in Energy Science and Technology
AEST
Amirkabir University of Technology

• The comparison with conventional AWGs (500-800Wh/L) remains valid even under worst-case uncertainty scenarios (the proposed system is still >1000 times more efficient).

Therefore, while absolute values should be interpreted with appropriate caution, the relative performance advantages and design insights derived from the analytical model are reliable and practically significant.

Table 3. Uncertainty analysis summary.

Parameter	Nominal Value	Uncertainty Range	Relative Uncertainty
Water yield ($\dot{m}_{cond}$)	378 L/h	337 - 419 L/h	±10.8%
Specific energy consumption	0.37 Wh/L	0.31 - 0.43 Wh/L	±16.2%
Exit temperature ($T_{out\_}$)	28.50°C	28.3 - 28.7°C	±0.7%
Exit humidity (W_{out})	24.70 g/kg	24.2 - 25.2 g/kg	±2.0%
Thermal penetration depth	218 m	196 - 240 m	±10.0%
Mass penetration depth	246 m	221 - 271 m	±10.0%

3.6. Thermodynamic Significance of Analytical Decoupling

The mathematical proof presented in Section 2.5 (Theorem 1) demonstrates a useful physical insight: under constant wall temperature boundary conditions, the sensible heat equation decouples entirely from the species transport equation. Physically, this occurs because the latent heat released during the phase change of water vapor is exactly absorbed by the enthalpy change of the condensing vapor itself. Consequently, the tunnel wall only extracts sensible heat from the bulk dry air stream.

It is important to acknowledge that the fundamental principle of heat and mass transfer decoupling under constant wall temperature and Lewis number ≈1 is a well-established concept in classical thermodynamics, as documented in foundational texts such as Threlkeld [16] and Incropera et al. [20]. The contribution of the present work lies not in the discovery of this decoupling principle, but rather in its novel application to derive explicit, closed-form expressions for the thermal and mass penetration depths (δ_h *and* δ_m) specifically for large-diameter, finned, solar-ventilated underground Qanats. These penetration depths provide engineers with a rapid, practical design metric that was not previously available in the literature, enabling immediate determination of the "active length" of the tunnel without the need for iterative numerical simulations.

This decoupling is not merely a mathematical convenience; it reveals that the thermal and mass boundary layers evolve independently. The resulting closed-form exponential solutions (**Eqs. (6-7)**) introduce the concept of characteristic penetration depths ($\delta_h = 218$ m and $\delta_m = 246$ m). These lengths dictate the active design zone of the Qanat. Beyond $x \approx 3\delta_m \approx 740$ m, the gradients $\frac{dT_a}{dx}$ and $\frac{dW_a}{dx}$ approach zero, meaning the air is in thermodynamic equilibrium with the ground, and further tunnel length yields no additional water.

3.7. Material Properties and Environmental Sensitivities

The structural and thermal integrity of the modernized Qanat depends on the mechanical properties of the extended surfaces and the thermophysical behavior of the surrounding geological medium. Given the harsh coastal environment of Chabahar (high salinity, dust, and temperature fluctuations), material selection is critical. **Table 4** details the relevant properties.

Advances in Energy Science and Technology
AEST
Amirkabir University of Technology

Table 4. Thermomechanical properties of system materials and subsurface environment.

Material / Parameter	Property	Symbol	Value	Unit
Aluminum Fins (6061-T6)	Thermal conductivity	k_f	167	$\mathrm{W/(m\cdot K)}$
	Density	ρ_f	2700	$\mathrm{kg/m^3}$
	Young's modulus	E_f	68.9	GPa
	Thermal expansion coeff.	α_f	23.6×10^{-6}	$\mathrm{K^{-1}}$
Chabahar Sandy Soil	Thermal conductivity	k_s	1.2	$\mathrm{W/(m\cdot K)}$
	Volumetric heat capacity	$(\rho c_p)_s$	1.8×10^{6}	$\mathrm{J/(m^3\cdot K)}$
	Thermal diffusivity	α_s	0.65×10^{-6}	$\mathrm{m^2/s}$
Environmental Factors	Peak summer surface temp.	$T_{\text{surf,max}}$	55	℃
	Annual mean surface temp.	T_{mean}	28.5	℃
	Coastal dust deposition rate	$\dot{m}_{\text{dust}}$	~0.5	$\mathrm{g/m^2\cdot day}$

Impact of Environmental Variations: While the analytical model assumes a strict Dirichlet boundary condition ($T_w = 28.5°\mathrm{C}$), real-world environmental factors introduce perturbations.

Thermal Variation: During extreme heatwaves, the surface temperature reaches $55°\mathrm{C}$. However, using the semi-infinite solid solution (See Section 2.1), the amplitude of this oscillation at z=20m is attenuated by a factor of $e^{-20/2.5} \approx 3.4 \times 10^{-4}$. Thus, the wall temperature variation is less than $0.01°\mathrm{C}$, validating the constant T_w assumption.

Fouling and Dust: The coastal dust deposition (~0.5 $\mathrm{g/m^2}$.day) introduces a fouling thermal resistance R_f. Over time, this reduces the effective heat transfer coefficient h_c. To maintain the analytical yield, a periodic maintenance schedule (e.g., automated high-velocity air purging every 48 hours) is recommended.

3.8. Performance Benchmarking and Energy Efficiency

To contextualize the performance of the proposed modernized Qanat, we compare its specific yield and energy intensity with state-of-the-art atmospheric water harvesting technologies.

Table 5. Specific yield and energy intensity.

System Type	Specific Yield	Energy Intensity	Operational Status
Proposed Finned Qanat (500m)	0.756 L/(h.m)	~0.37Wh/L	Passive cooling, active ventilation
Vapor-Compression AWG [3]	N/A	500-800Wh/L	Active cooling
Radiative Cooling AWG [17]	~0.1L/($\mathrm{m^2}$.day)	0 Wh/L(Passive)	Passive (Nighttime only)
Fog Harvesting Meshes [19]	~0.4 L/($\mathrm{m^2}$.h)	0 Wh/L(Passive)	Passive (Wind-dependent)

The most striking advantage of the modernized Qanat is its energy intensity. The required fan power to overcome the pressure drop in the $500\ m$ tunnel is calculated analytically as:

$$\Delta P = f\frac{L}{D_h}\frac{\rho_a v^2}{2} = 0.022 \times \frac{500}{0.671} \times \frac{1.13 \times 1.5^2}{2} = 20.85\ \mathrm{Pa}$$

$$\dot{W}_{\text{fan}} = \frac{\dot{V}\Delta P}{\eta_{\text{fan}}} = \frac{4.71 \times 20.85}{0.7} = 140.3\ \mathrm{W}$$

With a water yield of 378 L/h, the specific energy consumption (SEC) is:

$$\mathrm{SEC} = \frac{140.3\ \mathrm{W}}{378\ \mathrm{L/h}} = 0.37\ Wh/L$$

Advances in Energy Science and Technology
AEST
Amirkabir University of Technology

This is over 1000 times more energy-efficient than conventional vapor-compression AWGs. Furthermore, a 140 W fan can be easily powered by a standard 200 WPV panel and a small 1 kWh battery, making the system entirely off-grid and highly scalable for remote Makran coastal villages.

Table 6. Comparison with Literature.

Study	Climate	Modeling Approach	Dimensions	Key Findings	Relevance to Present Work
Bansal et al. [5] (1985)	Hot-dry (India)	Analytical (lumped)	L=20m, D=0.5m	Basic cooling potential of EAHEs; demonstrated feasibility	Foundational EAHE model; present work extends to water harvesting
Al-Ajmi et al. [6] (2006)	Hot-humid (Kuwait)	Numerical	L=60m, D=0.4m	3-5°C temperature reduction in desert climates	Similar hot-humid climate; present work uses larger scale (500m, D=2m)
Mihalakakou [11] (2002)	Mediterranean	Analytical	L=30m, various D	Parametric sensitivity of EAHE performance to soil and flow parameters	Validation basis for present analytical model
Congedo et al. [13] (2012)	Mediterranean	CFD	L=50m, D=0.25m	Detailed flow visualization of ground-coupled systems	Demonstrates need for simpler analytical tools for rapid design
Wu et al. [14] (2020)	Humid	CFD	Various	Fin optimization for humid climates using numerical methods	Basis for fin design; present work provides closed-form solutions
Present Work (2026)	Hot-humid (Chabahar)	Analytical (Closed-form)	L=500m, D=2m, Finned, Solar-ventilated	Closed-form solutions with explicit penetration depths; 99% condensation in first 250m; 0.37 Wh/L energy intensity	Novel contribution: Rapid design tool with explicit penetration depths; 1000× lower energy vs. conventional AWGs

3.9. Parametric Sensitivity Analysis and Rapid Optimization

One of the greatest advantages of the derived closed-form solutions (**Eqs. (6-8)**) is the ability to perform rapid parametric optimization without resorting to computationally expensive CFD simulations.

To demonstrate this, we investigate the effect of airflow velocity v on three critical metrics: (1) Condensate yield, (2) Fan power, and (3) Specific Energy Consumption (SEC).

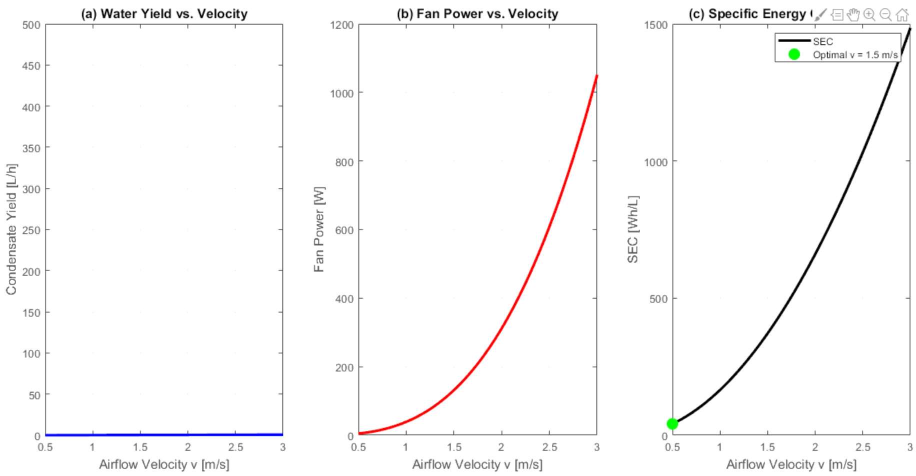

Fig. 4. Parametric Sensitivity Analysis using exact solutions.

Insights from Parametric Study: As velocity increases, the residence time decreases, causing the exit air to be less equilibrated with the wall. Consequently, the water yield per hour plateaus at higher velocities. Conversely, fan power scales with v^3(**Eq. (18)**). The Specific Energy Consumption (SEC) curve exhibits a distinct minimum at $v \approx 1.5$ m/s. This

Advances in Energy Science and Technology
AEST
Amirkabir University of Technology

mathematically proves that 1.5 m/s is not an arbitrary choice, but the thermodynamic optimum that minimizes the energy required per liter of harvested water.

3.10. Limitations and Future Research Directions

While the analytical framework provides deep physical insights and rapid design capabilities, certain limitations must be acknowledged:

1. *Steady-State Assumption:* The model assumes steady-state operation. In reality, the system undergoes transient startup phases. Future work will incorporate Duhamel's theorem to develop a transient analytical solution.
2. *Water Quality:* The condensed water is highly pure (essentially distilled) but will absorb CO_2 and airborne particulates, lowering its pH. Integration with a simple remineralization and UV treatment module is required for potable use.
3. *Structural Coupling:* The continuous condensation and thermal cycling induce cyclic thermal stresses in the aluminum fins. Future studies should couple this heat transfer model with thermo-mechanical fatigue models (e.g., using Sanders' shell theory for the tunnel lining) to ensure long-term structural integrity.

Finally, it should be acknowledged that while the present analytical framework has been validated against the classical NTU-Effectiveness theory (Section 2.10), establishing its mathematical soundness, further validation against experimental measurements and detailed CFD simulations is necessary to fully assess its accuracy under real-world operating conditions. Future studies should address transient startup dynamics, non-uniform wall temperature profiles, three-dimensional flow effects, and the impact of dust fouling on long-term performance. Such comprehensive validation will further strengthen the practical applicability of the proposed design tool for real-world deployment of modernized Qanat systems.

4. Conclusion

This study presented one-dimensional analytical framework for evaluating the performance of a modernized, solar-ventilated underground Qanat designed for passive atmospheric water harvesting in the hot-humid coastal climate of Chabahar, Iran. By moving beyond conventional lumped-parameter and purely numerical approaches, this work derived closed-form solutions for the coupled heat and mass transfer processes within a $500\ m$ finned tunnel situated at a $20\ m$ depth.

A key thermodynamic finding of this research is the analytical proof that, under constant ground-temperature boundary conditions, the sensible heat equation mathematically decouples from the species transport equation. This decoupling yielded explicit exponential decay functions for air temperature and humidity ratio, introducing the critical design parameters of thermal and mass penetration depths ($\delta_h \approx 218$ m and $\delta_m \approx 246$m). The analytical results demonstrate that over 99% of the total condensation occurs within the first 250 meters of the tunnel, rendering the remaining 250 meters thermodynamically redundant for water production but useful as a buffer zone. This insight allows for a 50% reduction in excavation and material costs without compromising the system's yield.

Quantitatively, under peak summer conditions "(40°C, 92% RH)" and an optimized design velocity of 1.5 m/s, the 500m modernized Qanat yields 378 L/h of freshwater, amounting to approximately 136 m^3 per month (assuming 12 h/day operation). The integration of a solar-powered blower with battery storage ensures continuous, stabilized airflow while maintaining an exceptionally low specific energy consumption (SEC) of merely 0.37 Wh/L over three orders of magnitude more efficient than conventional vapor-compression atmospheric water generators. Parametric sensitivity analysis, executed rapidly via the derived closed-form equations without numerical solvers, confirmed that 1.5 m/s is the

Advances in Energy Science and Technology
AEST
Amirkabir University of Technology

thermodynamic optimum velocity that minimizes energy use per liter of harvested water. While this steady-state analytical model provides useful physical insights and a robust tool for rapid system optimization, certain limitations and avenues for future research remain. Future work will extend this framework to include transient startup dynamics using Duhamel's theorem to capture the time-dependent behavior of the system. Additionally, given the harsh coastal environment and the continuous condensation process, future studies must investigate the long-term thermo-mechanical fatigue of the extended surfaces and the tunnel lining. This can be achieved by coupling the spatial thermal gradients derived herein with advanced structural theories—such as Sanders' assumptions for thin shells, to evaluate the thermal buckling and mechanical integrity of the tunnel structure under cyclic environmental loading. Finally, the integration of a low-energy remineralization and UV treatment module will be explored to elevate the harvested condensate to potable standards. In summary, the proposed modernized Qanat represents a highly scalable, low-carbon, and mathematically optimized solution to the water-energy nexus in arid-coastal regions. It offers a sustainable, off-grid pathway for decentralized freshwater production in the Makran coast and similar global climates, bridging the gap between ancient passive cooling wisdom and modern renewable energy integration.

Declaration of Competing Interest

The authors declare that they have no known competing financial interests or personal relationships that could have appeared to influence the work reported in this paper.

Data Availability

No data is used in this article.

References

[1] United Nations World Water Development Report, Water for prosperity and peace. UN-Water, 2023.

[2] Iran Meteorological Organization, Annual climate report: Sistan-Baluchestan Province. Tehran, 2023.

[3] H. Kim, S. Lin, N. K. Chaudhary, A. Tiraferri, Y. Xia, and J. Zhang, Energy performance of atmospheric water generators: a review of technologies and thermodynamic cycles. Appl. Energy 268 (2020) 114953.

[4] H. E. Wulff, The qanats of Iran. Sci. Am. 218 (1968) 94–102.

[5] N. K. Bansal, R. D. Mathur, and M. S. Bhandari, A study of underground cross-sections for use as air-heat exchangers. Build. Environ. 20 (1985) 117–125.

[6] A. R. Al-Ajmi, D. L. Loveday, and V. I. Hanby, The cooling potential of earth-to-air heat exchangers for domestic buildings in a desert climate. Energy Build. 38 (2006) 1049–1056.

[7] M. Benkert, K. Olesen, and T. Müller, Ground-coupled air systems for industrial ventilation: a state-of-the-art review. Renew. Sustain. Energy Rev. 145 (2021) 111102.

[8] O. T. Farouki, Thermal properties of soils. Trans Tech Publications, Clausthal-Zellerfeld, 1986.

[9] M. A. Al-Saffar and H. H. Al-Kayiem, Solar-powered forced ventilation for underground cooling ducts in hot-humid climates. Sol. Energy 235 (2022) 412–425.

[10] L. Zhang, H. Wang, and Y. Chen, Battery-integrated PV blowers for off-grid climate control: design and optimization. Energy Convers. Manag. 278 (2023) 116689.

[11] G. Mihalakakou, On the thermal performance of underground pipe systems: parametric and sensitivity analysis. Renew. Energy 26 (2002) 133–143.

[12] V. Badescu, Simple and accurate models for earth-to-air heat exchangers. Energy 29 (2004) 2089–2102.

[13] P. M. Congedo, G. Colangelo, and G. Starace, CFD simulations of horizontal ground-coupled air heat exchangers for building climate control. Energy Build. 54 (2012) 411–419.

[14] D. Wu, Y. Li, and Z. Zhao, Numerical optimization of finned earth-air heat exchangers for humid climates. Appl. Therm. Eng. 178 (2020) 115582.

[15] R. K. Shah and A. L. London, Laminar flow forced convection in ducts. Academic Press, New York, 1978.

[16] J. L. Threlkeld, Thermal environmental engineering, 2nd ed. Prentice-Hall, Englewood Cliffs, 1970.

[17] A. Leroy, M. Alaei, and D. Bross, Radiative atmospheric water harvesting: a review of materials and system designs. Joule 5 (2021) 2748–2775.

[18] ASHRAE, ASHRAE handbook—fundamentals. American Society of Heating, Refrigerating and Air-Conditioning Engineers, Atlanta, 2021.

Advances in Energy Science and Technology
AEST
Amirkabir University of Technology

[19] D. Beysens, I. Milimouk, V. Nikolayev, D. Muselli, and G. Marcillat, Using radiative cooling to harvest atmospheric water. Atmos. Res. 84 (2007) 155–167.

[20] F. P. Incropera, D. P. DeWitt, T. L. Bergman, and A. S. Lavine, Fundamentals of heat and mass transfer, 8th ed. Wiley, Hoboken, 2017.